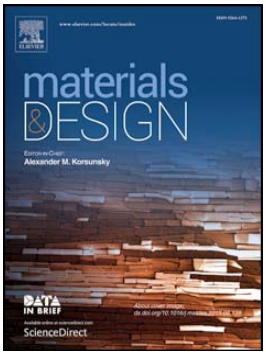

The effect of grain size on the annealing-induced phase transformation in an $Al_{0.3}CoCrFeNi$ high entropy alloy

Qunhua Tang, Yi Huang, Hu Cheng, Xiaozhou Liao, Terence G. Langdon, Pinqiang Dai

PII: S0264-1275(16)30674-8
DOI: doi: 10.1016/j.matdes.2016.05.079
Reference: JMADE 1827

To appear in:

Received date: 5 March 2016
Revised date: 2 May 2016
Accepted date: 19 May 2016

Please cite this article as: Qunhua Tang, Yi Huang, Hu Cheng, Xiaozhou Liao, Terence G. Langdon, Pinqiang Dai, The effect of grain size on the annealing-induced phase transformation in an $Al_{0.3}CoCrFeNi$ high entropy alloy, (2016), doi: 10.1016/j.matdes.2016.05.079

The effect of grain size on the annealing-induced phase transformation in an $Al_{0.3}CoCrFeNi$ high entropy alloy

Qunhua Tang [a,b], Yi Huang [c], Hu Cheng [a,d], Xiaozhou Liao [e,*], Terence G. Langdon [c,f], Pinqiang Dai [a,g,*]

[a] College of Materials Science and Engineering, Fuzhou University, Fuzhou 350108, China

[b] School of Mechanical & Electrical Engineering, Putian University, Putian 351100, China

[c] Materials Research Group, Faculty of Engineering and the Environment, University of Southampton, Southampton SO17 1 BJ, UK

[d] School of Mechanical Engineering, Taizhou University, Taizhou 318000, China

[e] School of Aerospace, Mechanical and Mechatronic Engineering, The University of Sydney, Sydney, NSW 2006, Australia

[f] Departments of Aerospace & Mechanical Engineering and Materials Science, University of Southern California, Los Angeles, CA 90089-1453, USA

[g] School of Materials Science and Engineering, Fujian University of Technology, Fuzhou 350108, China

[*] Corresponding authors: Tel: 61 2 9351 2348; Fax: 61 2 9351 7060; E-mail address: xiaozhou.liao@sydney.edu.au (Xiaozhou Liao), Tel: +86 591 22863280; fax: +86 591 22863279; E-mail address: pqdai@126.com (Pinqiang Dai)

Abstract

The annealing-induced phase transformation was investigated in coarse-grained and severely deformed nanocrystalline face-centered cubic (FCC) high entropy alloys (HEA). Increasing temperature leads to phase transformations from the FCC phase to an $L1_2$ phase and finally to a B2 phase in the coarse-grained HEA. By contrast, direct transformation from the FCC phase to the B2 phase was observed in the nanocrystalline HEA at a lower temperature.

Keywords: High entropy alloy; Nanocrystalline; Annealing; Phase transformation

1. Introduction

High entropy alloys (HEAs) are multi-component materials consisting of five or more principal elements with each elemental concentration between 5 at. % and 35 at. % [1]. Exhibiting a high mixing entropy, an HEA predominantly tends to form a simple solid solution with a face-centered cubic (FCC) phase, a body-centered cubic (BCC) phase or a mixture of the two phases rather than more complex intermetallic compounds [2]. HEAs are promising candidates for many structural applications due to their unusual properties, including high strength at ambient and elevated temperatures, reasonable ductility, excellent thermal stability and excellent resistance to oxidation [2-7]. These excellent properties are closely related to the structure and microstructure of HEAs that can be manipulated through various methods including heat treatments. Therefore, microstructural evolution and phase transformations induced by heat treatments in coarse-grained (CG, $\geq$1 μm) HEAs have been extensively investigated [8-13].

Refining grain sizes to the ultrafine (< 1 μm) and nanometer (< 100 nm) scales may lead to superior materials properties including a combination of high strength and reasonably good ductility [14, 15]. Severe plastic deformation (SPD) techniques including high-pressure torsion (HPT) have been widely used to produce ultrafine-grained (UFG) and nanocrystalline (nc) structures [16, 17]. It was reported that the grain size plays a significant role in affecting the phases and the phase transformations of these materials [18-20]. For example, a CG BCC

Ti-36Nb-2.2Ta-3.7Zr-0.3O alloy transformed to a hexagonal phase when it was deformed by HPT under a pressure of 3 GPa at room temperature. However, a reverse phase transformation from a hexagonal phase to a BCC phase occurred under the same deformation conditions when the grain sizes were less than 100 nm [18]. While a CG CoCrFeMnNi HEA with an FCC structure exhibits excellent high-temperature stability [21-24], the same alloy with an average grain size of ~50 nm produced by HPT would decompose at 723 K into three phases [5]. In an earlier report [25], it was shown that annealing of an HPT HEA with a composition of $Al_{0.3}$CoCrFeNi at 673 K for 1 h led to the formation of an ordered BCC secondary phase, which strengthens the material. However, the formation pathway of the secondary phase was not clearly defined and also it was not determined whether the grain size of the material affects the formation pathway. Accordingly, the present investigation was designed to compare the phase transformation processes of the HEA with CG and nc structures. The results show that a reduction in grain size to the nanometer scale significantly affects its heat treatment-induced phase transformation pathway.

2. Experimental procedures

An $Al_{0.3}$CoCrFeNi HEA ingot was prepared by vacuum induction melting of the constituent elements having at least 99.9 wt.% purity. The alloy was melted five times to improve its chemical homogeneity. The as-cast alloy was machined into discs with a diameter of 10 mm and a thickness of ~0.8 mm for HPT processing. The processing was performed at room temperature using a quasi-constrained HPT facility [26] under

an applied pressure of 6.0 GPa and a rotation rate of 1 rpm for 8 revolutions. Specimens with a diameter of 3 mm were cut from the edges of HPT discs for further investigation. Thermal analyses was performed using a NETZSCH 200F3 differential scanning calorimeter (DSC) over the temperature range of 308 to 843 K with a heating rate of 10 K/min in an Ar atmosphere. To investigate the microstructural evolution, samples were annealed for 1 h at temperatures determined by the DSC results. A transmission electron microscopy (TEM) investigation was performed using a JEM-2100 TEM operating at 200 kV equipped with an x-ray energy dispersive spectrometer (EDS). Compositional analysis was conducted using EDS by focusing the electron beam to a size much smaller than the sizes of the measured grains located at thin edges of the TEM foils. The count numbers in the EDS experiments were larger than 3000, implying that the statistical errors for compositional analysis were smaller than 1.8%. The grain sizes of the as-cast HEA measured from optical micrographs ranged from 100 um to 1100 um with the average size of ~ 350 um. The average grain size of the HPT HEA, which was obtained from bright-field TEM images by counting at least 200 grains along two orthogonal axes, was ~ 30 nm.

3. Results

Reducing the grain size from the micrometer to the nanometer scale leads to distinct differences in the DSC curves, as shown in Fig. 1. For the CG HEA, there is a small exothermic reaction starting from 600 K and with a peak at 639 K, followed by no significant change in heat flow over a broad temperature range. For the nc HEA, there is

a deep exothermic reaction starting from 593 K. To investigate the details of the heat treatment-induced phase transformations, the CG and nc HEA were annealed at 639 and 593 K, respectively. Although the DSC curves terminate at 843 K, annealing at a higher temperature was also conducted and the results are presented for both the CG and nc HEA annealed at 1123 K for 1 h.

Figs. 2 and 3 show microstructural evolution in CG samples induced by thermal annealing. The as-cast CG HEA contains only a single FCC phase. Figure 2a presents a typical $[001]_{FCC}$ selected-area electron diffraction (SAED) pattern of the FCC phase. The lattice constant measured from the SAED pattern is ~ 0.36 nm which is consistent with an earlier report of ~ 0.359 nm obtained from X-ray diffraction (XRD) [3]. Figure 2b shows a typical SAED pattern along the same direction from a sample annealed at 639 K. The appearance of {100} additional weak diffraction spots indicates the formation of an $L1_2$ ordered structure [8, 9]. A typical high-resolution TEM (HRTEM) image (Fig. 2c) of the annealed sample reveals a high density of spherical particles with dark contrast and a mean diameter of ~2 nm. The fast Fourier transformation (FFT) pattern and inverse FFT (IFFT) image inset in Fig. 2c in the upper left and right corners, respectively, were obtained from a spherical particle and its surrounding area highlighted by a white square in Fig. 2c. The {100} diffraction spots from the ordered $L1_2$ phase are circled in the FFT pattern and were used for the IFFT imaging. Note that the bright two-dimensional periodic lattice at the center of the IFFT image is from the $L1_2$ phase, while the surrounding dim lattice is artifact caused by the assumption of an infinite periodic lattice array in the IFFT calculation. The FFT and IFFT confirm that

the spherical particles in the annealed sample are of the $L1_2$ structure. As the spherical particles (the $L1_2$ phase) are distributed randomly and uniformly in the FCC matrix, it is believed that the $L1_2$ phase formed through a homogeneous nucleation process. This result indicates that the exothermic process with the DSC peak at 639 K in Fig.1 is caused by the formation of the $L1_2$ phase.

With increasing annealing temperature to 1123 K, the average size of the spherical particles increased significantly to ~ 20 nm and lath-like particles with lengths of ~ 44 nm and widths of ~ 15 nm were formed, as shown in Fig. 3. The SAED pattern in Fig. 3b suggests the $L1_2$ phase of the spherical particles, while the SAED pattern in Fig. 3c demonstrates that the lath-like particles are of a B2 ordered BCC structure with a lattice constant of ~ 0.29 nm which is consistent with the reported XRD data of ~ 0.288 nm for the B2 NiAl phase in $Al_xCoCrFeNi$ HEA [4].

Figure 4 shows a typical microstructure of the nc HEA. The nc HEA is of equiaxed grains with a grain size range of ~ 10 to ~ 80 nm and an average grain size of ~30 nm. Only grains showing clear grain boundaries in TEM images were counted for the grain size measurement and multiple TEM images from the same area were taken under different specimen tilting conditions to include as many grains with clear boundaries as possible. The SAED pattern inset in Fig. 4 shows fairly uniform rings that are indexed based on the single FCC structure. The average grain size of the nc HEA remains unchanged after annealing at 593 K. An HRTEM image of a nanograin in Fig. 5a reveals Moiré fringes with spacing of ~ 1.7 nm in the vicinity of the grain boundaries.

The FFT pattern in Fig. 5b, taken from the area marked by the white square in Fig. 5a, presents two sets of reciprocal space lattices that are indexed as a $<011>_{FCC}$ and a $<111>_{BCC}$, respectively, based on the interplanar distances and planar orientations deduced from the diffraction spots. This means that these Moiré fringes in Fig. 5a are caused by the overlapping of two crystal lattices with FCC and BCC structures along the electron beam direction. Indexing of the FFT pattern suggests the Kuridjumov-Sachs orientation relationship of $<110>_{FCC}//<111>_{BCC}$ and $\{111\}_{FCC}//\{110\}_{BCC}$ [27]. Annealing at 1123 K led to significant grain growth. The average grain sizes of the FCC and the BCC phases reached ~ 840 nm and ~ 250 nm, respectively, as shown in Fig. 6. No new phase was formed. The SAED pattern inset in Fig. 6 reveals that the secondary phase with black contrast is of the B2 ordered BCC structure which is consistent with earlier results [25].

Careful examination of the nc HEA annealed at 593 K showed no evidence for the $L1_2$ phase. Extra annealing experiments at 523 K and 573 K, which are slightly lower than the exothermic starting temperature, showed only the FCC phase in this alloy. Thus, it is clear that the formation of the B2 phase is the major contributor for the exothermic process in the nc HEA starting from 593 K. No $L1_2$ phase formed during the annealing process of the nc HEA.

Table 1 lists the chemical compositions of phases in the CG and nc samples. The measured composition of the FCC phase in the as-cast CG sample matches very well with the nominal composition of the HEA, thereby suggesting reasonably good

accuracy for the EDS analysis. Both the $L1_2$ and B2 phases in the CG sample annealed at 1123 K contain more Al and Ni but less Co, Cr and Fe than the FCC matrix. Comparing the compositions in the FCC matrix, the $L1_2$ and B2 phases show that the content of each element in the three phases increases or decreases monotonously, suggesting that less elemental diffusion is needed for the formation of the $L1_2$ phase than for the formation of the B2 phase. The compositions of the FCC matrix and the B2 phase in nc HEA annealed at 1123 K are similar to those in the CG materials annealed at 1123 K (see table 1).

4. Discussion

For the CG HEA, an annealing-induced phase transformation occurs through the following sequence: the supersaturated FCC phase $\rightarrow$ the $L1_2$ phase $\rightarrow$ the B2 phase. Increasing the annealing temperature involves in part a decomposition of the supersaturated solid solution which commences with the formation of the $L1_2$ phase. At higher temperatures, the $L1_2$ phase is replaced by the formation of the B2 phase. For the nc HEA, the annealing-induced phase transformation does not include the formation of the $L1_2$ phase and the formation of the B2 phase occurs directly from the supersaturated FCC phase at a lower temperature compared with the CG HEA. It is worth noting that the FCC phase is still available in both CG and nc HEA after annealing.

The difference in the phase transformation pathway may be correlated with the phase formation mechanism. The formation of the $L1_2$ phase in a CG FCC-based HEA effectively reduces the lattice distortion caused by the atomic size difference among the

constituent elements [9] since the CG HEA reported here comprises five elements with different atomic radii (Al, 0.143 nm; Co, 0.128 nm; Cr, 0.130 nm; Fe, 0.128 nm; and Ni, 0.128 nm) [28]. The formation of the $L1_2$ phase, which started from a short-range elemental rearrangement [29] followed by some long-range elemental diffusion that leads to the formation of the B2 phase, is kinetically more favorable at relatively low annealing temperatures than the formation of the B2 phase.

The ordering in the FCC phase originates from the selective occupation of Al to form an M_3Al-type $L1_2$ phase where M denotes the mixture of multicomponents in the HEA by randomly substituting Ni atoms in the typical $L1_2$ compound Ni_3Al [9]. The lowest mixing enthalpy of Al-Ni among all the atomic pairs in the HEA provides a thermodynamic driving force for the formations of phases rich in Al and Ni atoms. In addition, the oversized substitutional element of Al imposes strain in its vicinity and introduces additional stress energy. Therefore, Al segregation from the FCC matrix minimizes the system free energy. Because the formation of the B2 phase requires significant long-distance atomic diffusion and because HEAs usually possess a sluggish diffusion effect [22], the formation of the B2 phase in the CG HEA occurs only at elevated temperatures when the kinetic condition is fulfilled. By contrast, the large grain boundary volume fraction in the nc HEA provides a pathway for rapid long-distance elemental diffusion along grain boundaries even at relatively low temperatures, as reported in Ref. [5]. This allows the direct formation of the B2 phase at or near grain boundaries at a relatively low temperature that would allow only relatively short-distance diffusion for the $L1_2$ formation in CG HEAs. Thus, at temperatures that

kinetically allow short-distance diffusion for the formation of the $L1_2$ phase in CG HEAs, long-distance diffusion occurs already through the grain boundaries and this permits the formation of the B2 phase without introducing the $L1_2$ phase. Finally, although the density of vacancies in severely deformed materials is very high, this will not affect the phase transformation in the nc HEA as the annealing temperature of 593 K is sufficiently high that non-equilibrium vacancies are annihilated.

5. Conclusions

The annealing-induced phase transformation processes are different in the CG and nc HEA. This is due to the difference in elemental diffusivity in CG and nc materials. The grain boundaries in the nc HEA provide a pathway for rapid elemental diffusion that allows the formation of a high-temperature stable B2 phase at a relatively low temperature and therefore suppresses the formation of the $L1_2$ phase.

Acknowledgements

This work was supported by Fujian University of Technology (Grant No. E0600133), the European Research Council (Grant No. 267464-SPDMETALS), the public technology applied research projects of Zhejiang Province (Grant No. 2013C31117), and the Australian Research Council (Grant No. DP150101121).

References

[1] J.W. Yeh, S.K. Chen, S.J. Lin, J.Y. Gan, T.S. Chin, T.T. Shun, C.H. Tsau, S.Y. Chang, Nanostructured High-Entropy Alloys with Multiple Principal Elements: Novel Alloy Design Concepts and Outcomes, Adv. Eng. Mater. 6 (2004) 299-303.

[2] Y. Zhang, T.T. Zuo, Z. Tang, M.C. Gao, K.A. Dahmen, P.K. Liaw, Z.P. Lu, Microstructures and properties of high-entropy alloys, Prog. Mater. Sci. 61 (2014) 1-93.

[3] S.G. Ma, S.F. Zhang, J.W. Qiao, Z.H. Wang, M.C. Gao, Z.M. Jiao, H.J. Yang, Y. Zhang, Superior high tensile elongation of a single-crystal $CoCrFeNiAl_{0.3}$ high-entropy alloy by Bridgman solidification, Intermetallics 54 (2014) 104-109.

[4] C. Li, J.C. Li, M. Zhao, Q. Jiang, Effect of aluminum contents on microstructure and properties of $Al_xCoCrFeNi$ alloys, J. Alloy. Compd 504, Supplement 1 (2010) S515-S518.

[5] B. Schuh, F. Mendez-Martin, B. Völker, E.P. George, H. Clemens, R. Pippan, A. Hohenwarter, Mechanical properties, microstructure and thermal stability of a nanocrystalline CoCrFeMnNi high-entropy alloy after severe plastic deformation, Acta Mater. 96 (2015) 258-268.

[6] F. Otto, A. Dlouhý, C. Somsen, H. Bei, G. Eggeler, E.P. George, The influences of temperature and microstructure on the tensile properties of a CoCrFeMnNi high-entropy alloy, Acta Mater. 61 (2013) 5743-5755.

[7] B. Gorr, M. Azim, H.J. Christ, T. Mueller, D. Schliephake, M. Heilmaier, Phase equilibria, microstructure, and high temperature oxidation resistance of novel refractory high-entropy alloys, J. Alloy. Compd 624 (2015) 270-278.

[8] T. Shun, Y. Du, Microstructure and tensile behaviors of FCC $Al_{0.3}$CoCrFeNi high entropy alloy, J. Alloy. Compd 479 (2009) 157-160.

[9] X.D. Xu, P. Liu, S. Guo, A. Hirata, T. Fujita, T.G. Nieh, C.T. Liu, M.W. Chen, Nanoscale phase separation in a fcc-based CoCrCuFeNi$Al_{0.5}$ high-entropy alloy, Acta Mater. 84 (2015) 145-152.

[10] H.R. Sistla, J.W. Newkirk, F. Frank Liou, Effect of Al/Ni ratio, heat treatment on phase transformations and microstructure of Al_xFeCoCrNi_{2-x} (x = 0.3, 1) high entropy alloys, Mater. Design 81 (2015) 113-121.

[11] L.C. Tsao, C.S. Chen, C.P. Chu, Age hardening reaction of the $Al_{0.3}CrFe_{1.5}MnNi_{0.5}$ high entropy alloy, Mater. Design 36 (2012) 854-858.

[12] Y. Dong, L. Jiang, H. Jiang, Y. Lu, T. Wang, T. Li, Effects of annealing treatment on microstructure and hardness of bulk AlCrFeNi$Mo_{0.2}$ eutectic high-entropy alloy, Mater. Design 82 (2015) 91-97.

[13] N.G. Jones, R. Izzo, P.M. Mignanelli, K.A. Christofidou, H.J. Stone, Phase evolution in an $Al_{0.5}$CrFeCoNiCu High Entropy Alloy, Intermetallics 71 (2016) 43-50.

[14] R.Z. Valiev, I.V. Alexandrov, Y.T. Zhu, T.C. Lowe, Paradox of Strength and Ductility in Metals Processed Bysevere Plastic Deformation, J. Mater. Res. 17 (2002) 5-8.

[15] M.A. Meyers, A. Mishra, D.J. Benson, Mechanical properties of nanocrystalline materials, Prog. Mater. Sci. 51 (2006) 427-556.

[16] D. Lee, I. Choi, M. Seok, J. He, Z. Lu, J. Suh, M. Kawasaki, T.G. Langdon, J. Jang, Nanomechanical behavior and structural stability of a nanocrystalline CoCrFeNiMn

high-entropy alloy processed by high-pressure torsion, J. Mater. Res. 30 (2015) 2804-2815.

[17] A.P. Zhilyaev, T.G. Langdon, Using high-pressure torsion for metal processing: Fundamentals and applications, Prog. Mater. Sci. 53 (2008) 893-979.

[18] Y.B. Wang, Y.H. Zhao, Q. Lian, X.Z. Liao, R.Z. Valiev, S.P. Ringer, Y.T. Zhu, E.J. Lavernia, Grain size and reversible beta-to-omega phase transformation in a Ti alloy, Scripta Mater. 63 (2010) 613-616.

[19] K. Edalati, T. Daio, M. Arita, S. Lee, Z. Horita, A. Togo, I. Tanaka, High-pressure torsion of titanium at cryogenic and room temperatures: Grain size effect on allotropic phase transformations, Acta Mater. 68 (2014) 207-213.

[20] Y.B. Wang, X.Z. Liao, Y.H. Zhao, J.C. Cooley, Z. Horita, Y.T. Zhu, Elemental separation in nanocrystalline Cu-Al alloys, Appl. Phys. Lett. 102 (2013) 231912.

[21] B. Cantor, I.T.H. Chang, P. Knight, A.J.B. Vincent, Microstructural development in equiatomic multicomponent alloys, Materials Science and Engineering: A 375 – 377 (2004) 213-218.

[22] K.Y. Tsai, M.H. Tsai, J.W. Yeh, Sluggish diffusion in Co−Cr−Fe−Mn−Ni high-entropy alloys, Acta Mater. 61 (2013) 4887-4897.

[23] F. Otto, Y. Yang, H. Bei, E.P. George, Relative effects of enthalpy and entropy on the phase stability of equiatomic high-entropy alloys, Acta Mater. 61 (2013) 2628-2638.

[24] M. Laurent-Brocq, A. Akhatova, L. Perrière, S. Chebini, X. Sauvage, E. Leroy, Y. Champion, Insights into the phase diagram of the CrMnFeCoNi high entropy alloy, Acta Mater. 88 (2015) 355-365.

[25] Q.H. Tang, Y. Huang, Y.Y. Huang, X.Z. Liao, T.G. Langdon, P.Q. Dai, Hardening of an $Al_{0.3}$CoCrFeNi high entropy alloy via high-pressure torsion and thermal annealing, Mater. Lett. 151 (2015) 126-129.

[26] R.B. Figueiredo, P.R. Cetlin, T.G. Langdon, Using finite element modeling to examine the flow processes in quasi-constrained high-pressure torsion, Materials Science and Engineering: A 528 (2011) 8198-8204.

[27] G. Kurdjumov, G. Sachs, Über den Mechanismus der Stahlhärtung, Z. Phys. 64 (1930) 325-343.

[28] T. Egami, Y. Waseda, Atomic size effect on the formability of metallic glasses, J. Non-Cryst. Solids 64 (1984) 113-134.

[29] Y.R. Wen, Y.P. Li, A. Hirata, Y. Zhang, T. Fujita, T. Furuhara, C.T. Liu, A. Chiba, M.W. Chen, Synergistic alloying effect on microstructural evolution and mechanical properties of Cu precipitation-strengthened ferritic alloys, Acta Mater. 61 (2013) 7726-7740.

Figure captions

Fig. 1 DSC curves for the CG and nc HEA

Fig. 2 (a) An SAED pattern obtained from the as-cast HEA; (b) an SAED pattern obtained from the CG HEA annealed at 639 K; (c) an HRTEM image from the CG HEA annealed at 639 K; the white square in (c) indicates the area from which the inset FFT pattern and IFFT image were obtained.

Fig. 3 (a) A TEM image from the CG HEA annealed at 1123 K; (b) an SAED pattern obtained from a spherical particle; (c) an SAED pattern obtained from a lath-like particle.

Fig. 4 A typical TEM image and its corresponding SAED pattern of the nc HEA.

Fig. 5 (a) An HRTEM image of a nanoscale grain from the nc HEA annealed at 593 K; (b) FFT patterns corresponding to the white square area in (b).

Fig. 6 A TEM image from the nc HEA annealed at 1123 K, the inset SAED pattern was obtained from a particle with black contrast.

Table 1 Chemical compositions of phases in the HEA obtained by EDS (at.%)

Sample	Phase	Al	Co	Cr	Fe	Ni
Nominal Composition		6.96	23.26	23.26	23.26	23.26
CG (as-cast)	FCC	6.8	23.7	22.6	23.1	23.8
CG (1123 K)	FCC	4.3	23.2	27.6	23.5	21.4
	$L1_2$	11.8	19.2	10.7	16.2	42.1
	B2	30.9	11.4	6.1	9.3	42.3
nc (1123 K)	FCC	3.1	24.5	27.1	25.3	20.0
	B2	34.5	12.7	5.8	9.7	37.3

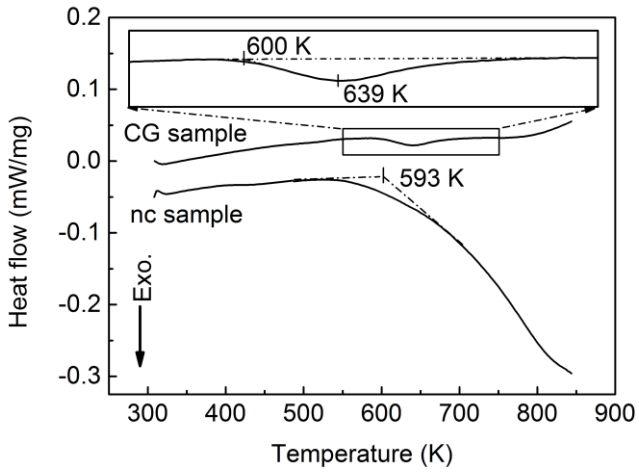

Figure 1

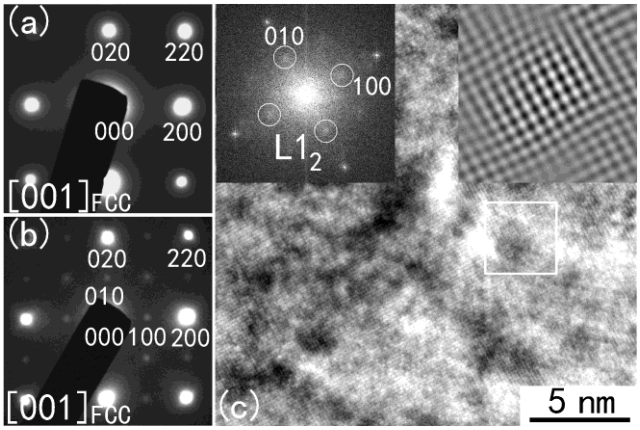

Figure 2

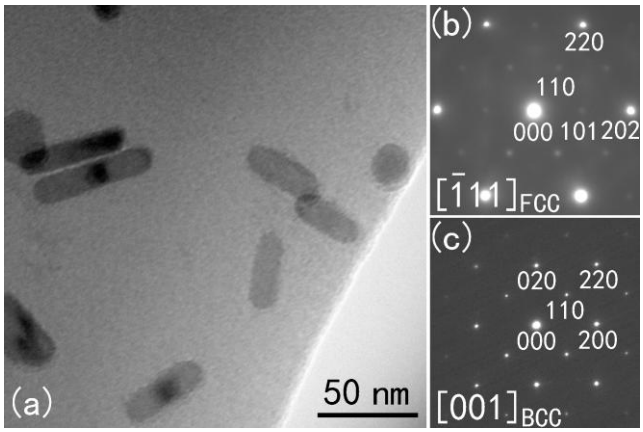

Figure 3

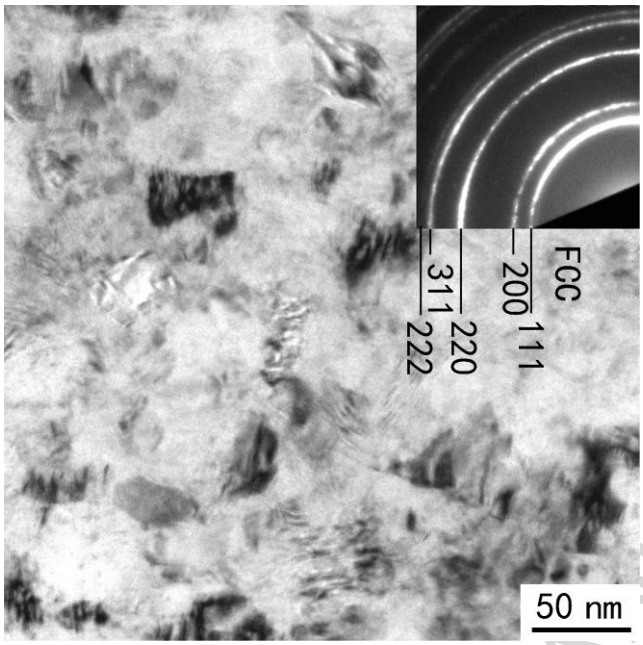

Figure 4

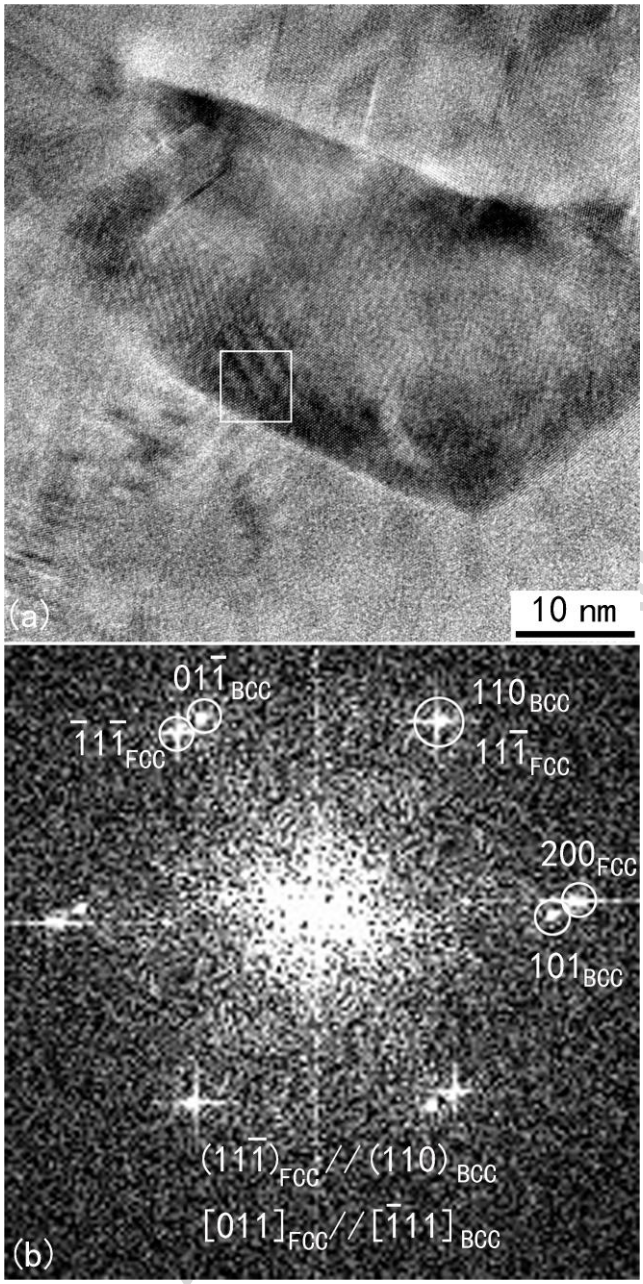

Figure 5

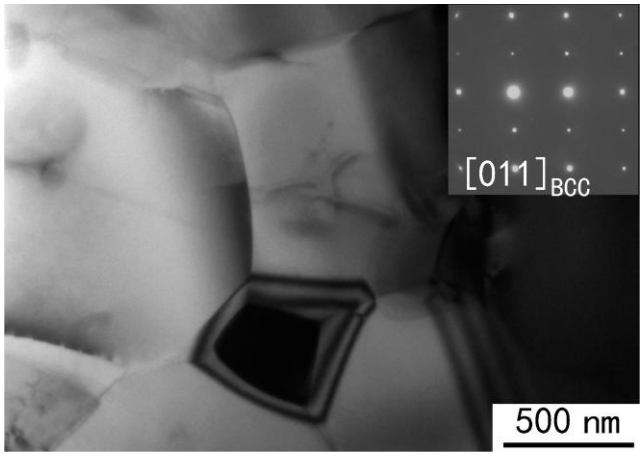

Figure 6

Graphical abstract

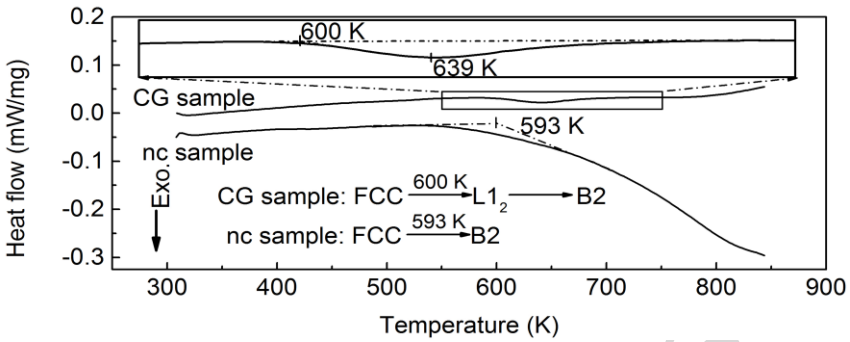

Highlights

- Grain size affects annealing-induced phase transformations in $Al_{0.3}CoCrFeNi$.
- Coarse-grained alloy transforms from FCC to $L1_2$ and finally to B2.
- Nanocrystalline alloy transforms from FCC directly to B2.
- Rapid elemental diffusion via grain boundaries in nanocrystalline alloy suppresses $L1_2$ formation.